Renewable Energy 215 (2023) 119003

Contents lists available at ScienceDirect

Renewable Energy

journal homepage: www.elsevier.com/locate/renene

Validation of a biomass conversion mechanism by Eulerian modelling of a fixed-bed system under low primary air conditions

César Álvarez-Bermúdez [a,*], Andrés Anca-Couce [b,c], Sergio Chapela [a], Robert Scharler [b], Markus Buchmayr [d], Miguel Ángel Gómez [a], Jacobo Porteiro [a]

[a] CINTECX, Universidade de Vigo, Grupo de Tecnología Energética (GTE), 36310, Vigo, Spain
[b] Graz University of Technology, Institute of Thermal Engineering, Inffeldgasse 25/B, 8010, Graz, Austria
[c] Carlos III University of Madrid, Thermal and Fluids Engineering Department, Avda. de la Universidad 30, 28911, Leganés, Madrid, Spain
[d] Hargassner GesmbH, Anton Hargassner Straße 1, 4952, Weng, Austria

ARTICLE INFO

Keywords:
Biomass combustion
Fixed bed
Pyrolysis
Computational fluid dynamics
Eulerian modelling

ABSTRACT

This work presents a three-dimensional Computational Fluid Dynamics study of a small-scale biomass combustion system operating with low primary air ratios. The Eulerian Biomass Thermal Conversion Model (EBiTCoM) was adapted to incorporate a pyrolysis mechanism based on the detailed Ranzi-Anca-Couce (RAC) scheme. Two scenarios were simulated using woodchips with 8% and 30% moisture content, and the results were validated against experimental data, including in-flame and bed measurements. The model accurately predicted bed temperature profiles and the influence of fuel moisture content on the pyrolysis and drying fronts, as well as on the distribution of volatiles and temperatures above the solid fuel bed. For the 8% moisture content case, the average gas temperature above the bed is approximately 700 °C, while for the 30% case, it drops to around 400 °C. The lower temperatures hinder the tar cracking reaction, resulting in a 25% higher tar content in the producer gas for the 30% moisture content fuel. The lower part of the bed consists of a thick layer of char undergoing reduction reactions, similar to that of an updraft gasifier. The developed model can accurately simulate biomass combustion systems with solid fuel beds consisting of numerous particles, while maintaining low computational requirements.

1. Introduction

Heat production accounts for the largest share of end-use energy, and most of this demand (72.5% in 2019) is met by fossil fuels [1]. Biomass can be a great substitute for fossil fuels in order to reduce greenhouse gases emissions while also helping to increase countries' energy independence [2,3]. The direct combustion of solid biomass is the simplest and, consequently, the predominant option for heat and electricity production from biomass resources [1–3]. However, during the combustion of solid biomass, polluting and harmful emissions such as particulate matter (PM), hydrocarbons, carbon monoxide (CO) or nitrogen oxides (NOx) are produced [4]. Furthermore, the presence of inorganic compounds in biomass fuel can result in ash-related problems such as fouling, slagging, and corrosion, leading to reduced thermal efficiency and damage to combustion systems [5–9]. In addition, the use of low-grade biomass fuels can further exacerbate these problems [10,11].

Experimental assessments of various biomasses in multi-fuel commercial boilers have demonstrated a direct relationship between the nitrogen content of the fuel and NOx emissions [11,12]. Furthermore, it has been observed that fuels containing higher amounts of inorganic compounds, such as potassium and phosphorus, tend to produce increased PM emissions [12]. Hence, it is necessary to utilize emissions abatement systems and enhance boiler design to meet emissions criteria [12,13]. Primary measures, such as air staging, can be applied to reduce emissions in biomass combustion systems. Experimental tests conducted in lab-scale biomass combustors have found that a proper distribution of secondary air staging can lead to a decrease in both CO and PM emissions [14,15]. Similarly, studies on commercial small-scale boilers have also demonstrated that implementing air staging and regulating air excess can effectively reduce both PM emissions [16,17] and NOx emissions [17–19]. Additionally, reducing the primary air ratio can decrease CO [18] and PM [16] emissions. However, these techniques typically involve a trade-off between NOx and CO emissions [15,19–21], and fuel flexibility remains limited, particularly in small-scale biomass

* Corresponding author.
E-mail address: cesalvarez@uvigo.gal (C. Álvarez-Bermúdez).

https://doi.org/10.1016/j.renene.2023.119003
Received 1 September 2022; Received in revised form 14 June 2023; Accepted 6 July 2023
Available online 6 July 2023

boilers and stoves [22].

With the aim of developing a small-scale multi-fuel low-emission biomass boiler, several experimental studies showcasing a novel biomass combustion technology capable of operating with low primary air ratios were presented [23–25]. The oxygen-limited regime in the fixed bed results in a thermal behaviour similar to a gasifier, with lower maximum temperatures than a typical combustion system [23,25–27]. This minimizes the volatilization of ash-forming elements, which, combined with lower gas velocities in the bed, results in a reduction of PM emissions [23,25,28], allowing a wider fuel flexibility.

To gain a better understanding of the complex thermal conversion phenomena occurring inside a biomass combustion system, numerical modelling techniques can be applied. Computational Fluid Dynamics (CFD) tools are widely used to simulate biomass combustion systems of various scales, enabling the improvement of design, efficiency, and the study of biomass combustion phenomena [29–34]. While CFD codes can solve the gas phase, models are needed to characterize the thermal conversion of biomass fuel. The Eulerian Biomass Thermal Conversion Model (EBiTCoM), developed by the GTE research group of the University of Vigo, is a porous-media based model that has been extensively used to simulate biomass fixed-bed combustion systems, from experimental [35,36] and domestic [37,38] systems to industrial plants [39]. In these cases, typical air-staging conditions with primary excess air ratios higher than 0.5 were studied. However, in this new scenario of low primary air ratios, the pyrolysis reaction gains particular significance due to the limited availability of oxygen in the primary zone.

Pyrolysis is the thermal degradation of solid biomass at temperatures ranging from 300 to 600 °C, either in the absence of oxygen or with a restricted oxygen supply [40]. This process leads to the decomposition of biomass into solid char, condensable tars (also known as bio-oil), and volatile gases [40]. When modelling pyrolysis in CFD simulations of biomass combustion systems, it is essential to have an accurate description of the pyrolysis reaction rate as well as the yields and compositions of the reaction products. In the literature, several common approaches can be found. Some authors consider the dry wood as a lumped artificial specie, with its composition based on the proximate and ultimate analysis of the fuel. They model pyrolysis as a single step and first order reaction [29,32] or as the sum of three competing reactions with different reaction products (gas, tar and char) [41,42]. Other authors consider the decomposition of wood pseudo-components (cellulose, hemicellulose and lignin) with a kinetic rate for each component [43,44]. The reaction rates are typically described by Arrhenius equations, where the pre-exponential factors and activation energies are obtained experimentally for different fuels using techniques such as thermogravimetric analysis. Regarding the composition of volatiles, the most common methods involve using data from experimental measurements as input for the simulation [30] or obtaining a volatile distribution based on elemental and energy balances [34,43,45]. However, these methods, either based on empirical correlations or detailed product composition, have limitations in terms of their applicability and accuracy. The Ranzi-Anca-Couce (RAC) is a detailed reaction scheme that considers the contributions of cellulose, hemicellulose, and lignin in pyrolysis [46,47]. This model has demonstrated its suitability in describing the product composition in various processes, including fixed-bed pyrolysis [48], fixed-bed torrefaction [49] and fixed-bed updraft gasification [50], where secondary charring reactions play a crucial role.

While a composition of pyrolysis products derived from the RAC scheme has been previously evaluated through one-dimensional modelling [50], its implementation in a detailed three-dimensional framework allows for the assessment of its accuracy in predicting the spatial distribution of conversion zones within the fixed bed, as well as temperatures and released volatiles. For this purpose, the EBiTCoM biomass thermal conversion mechanism will be modified to incorporate a pyrolysis description for softwood derived from the application of the RAC scheme. To validate the model and asses the accuracy of the pyrolysis description, the previously mentioned novel small-scale multi-fuel biomass boiler [23] will be simulated. Two different cases will be studied. One case corresponds to an experimental test using woodchips with an 8% moisture content, while the other corresponds to woodchips with a 30% moisture content. The simulations will be validated against experimental data, which includes temperature measurements inside the fixed bed, temperature measurements above the fixed bed, and the spatial distribution of gas species above the solid fuel bed [23]. The gas composition measurements in the flame zone are not common. In most biomass boiler studies, gas extractions are taken downstream of the secondary combustion zone, such as at the system outlet, where the species have been fully, or almost completely, oxidized. In this case, the measurements are taken above the bed surface, prior to secondary combustion, thus enabling a more precise evaluation of the pyrolysis mechanism and verification of the accuracy of predicted reaction zones. The data obtained from the simulations will be utilized to analyse the various processes occurring during the combustion of the biomass fuel under low primary air conditions. In addition, the impact of fuel moisture content on its thermal conversion will be examined.

2. Model

The simulations are conducted using ANSYS-Fluent version 19.2, a commercial software capable of modelling gas phase phenomena including fluid flow, heat transfer, species transport, and homogeneous reactions [29–32,36,39,45]. To characterize the thermal conversion of biomass fuel, the EBiTCoM model is utilized. This model is a three-dimensional transient model that is fully integrated with the CFD code as a User Defined Function (UDF) written in C/C++. An overview of the iterative calculation procedure of the numerical simulation is included in Fig. 1. For each time-step, the model first adjusts parameters such as material properties, reaction rates, or source terms based on the previous solution. It then iteratively solves the different equations until the solution converges. Once that is achieved, the fuel feeding algorithms and bed physics are executed, and the process starts over again. This leads to a transient calculation, which may or may not converge to a pseudo-steady-state solution.

2.1. Solid phase

The solid fuel bed is modelled as a porous disperse medium. The cell-zones where solid fuel particles may exist are set as porous zones. The properties of the solid are characterized using User Defined Scalars (UDS), which represent local volume-averaged values for each cell. Seven scalars are used to characterize the solid fuel. The solid fraction scalar (ε) represents the volumetric fraction of the cell that is occupied by solid fuel. A cell without any solid fuel will have a solid fraction value of 0 (porosity equal to 1). The bed cells cannot be entirely filled with solid, as the solid fuel will have a maximum compaction limit. The density scalars for moisture (ρ_{mois}), wood (ρ_{wood}), char (ρ_{char}) and ash (ρ_{ash}) define the composition of the solid volume within each cell. The average size of the solid fuel particles is represented by the third power of the cube of the average equivalent diameter of the particles (d^3_{eq}).

Regarding the temperature of the solid fuel volume, the bed model is based on a thermally thin assumption. This assumption considers the solid as a homogeneous mixture of solid fuel components with a homogeneous temperature (T_S) throughout the entire solid volume of each cell. In certain cases, a thermally thick assumption could provide more accuracy by considering temperature gradients within the particles. However, implementing a thermally thick assumption would come with higher computational costs, as it would require accounting for multiple layers within each particle with different temperatures [51,52].

The transient evolution of the scalars is defined by seven transport equations [35,36,39]. The solid densities equations consider the consumption and generation ratios of the wood components associated with each scalar. Similarly, the transient evolution of the solid fraction and

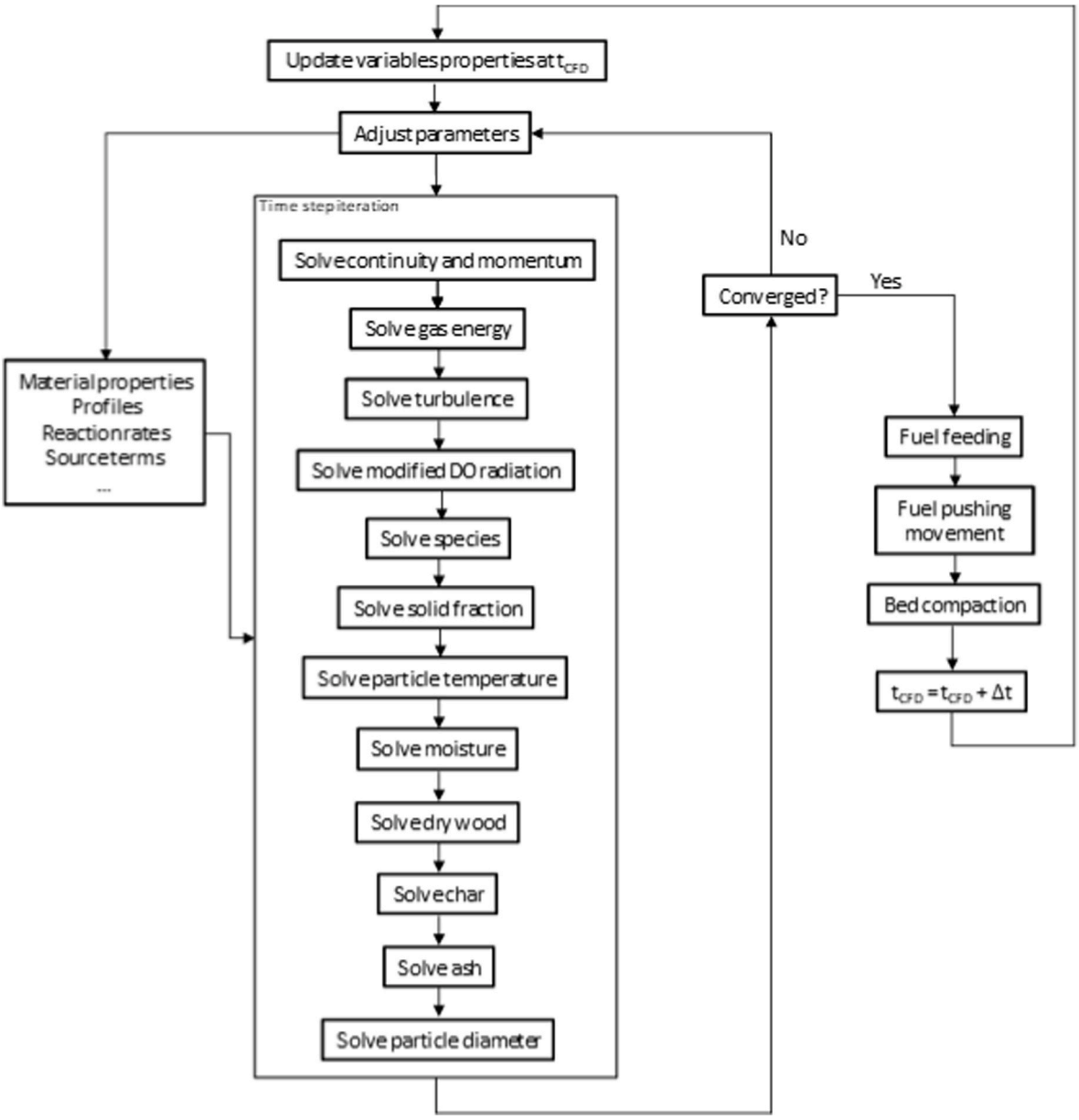

Fig. 1. Overview of EBiTCoM solution algorithm.

particle equivalent diameter depends on the wood and char consumption and generation ratios [35]. The temperature of the solid is calculated in function of the evolution of its enthalpy. The corresponding equation includes a diffusive term to account for heat conduction through the solid and a source term to consider the energy gains or losses resulting from reactions (drying, pyrolysis and char reactions) and heat transfer by convection and radiation [35]. The effective thermal conductivity of the solid is calculated as the mass-weighted average sum of the thermal conductivities of the moisture and solid components [35]. An experimental correlation for heat transfer in packed beds is used to obtain the convective heat transfer coefficient [53]. The same method is applied to obtain the mass transfer coefficients [54]. The radiation heat exchange between the solid phase and gas phase is modelled by a modified version of the Discrete Ordinates radiation model [55].

The ash is non-reactive but it can be compacted when the solid fuel collapses due to the shrinkage of the particles [35]. Furthermore, bed movement physics algorithms are implemented to simulate the movement of the solid fuel bed. These algorithms account for bed compaction and replicate the behaviour of granular materials, which tend to form a pile with a characteristic angle of repose [56,57]. A fuel feeding algorithm was applied to replicate the effect of a screw-conveyor introducing fresh fuel into the system through the fuel inlet [39].

2.2. Solid phase reactions

In Table 1, the equations of the consumption and generation rates of the moisture and solid components are shown.

The drying of the fuel initiates when the solid reaches a temperature

Table 1
Moisture and solid components consumption and generation rates.

Drying rate	$\dot{\omega}''_{moisture} = \tau \frac{\rho_P C_p}{LH_{moisture}} \frac{\partial T_S}{\partial t}, T_S \geq T_{evap}$
Pyrolysis rate	$\dot{\omega}''_{wood} = \rho_{wood} \cdot K^{pyr}$
Char consumption rate	$\dot{\omega}''_{C,char} = K^{ox}_{glob} A_v [O_2] M_{char} + K^{g,1}_{glob} A_v [CO_2] M_{char} + K^{g,2}_{glob} A_v [H_2O] M_{char}$
Char generation rate	$\dot{\omega}''_{G,char} = 0.2336 \cdot \rho_{wood} \cdot K^{pyr}$

Table 2
Solid phase reactions (stoichiometry in mass fraction for pyrolysis and mol fraction for char reactions).

Pyrolysis	Kinetic [1/s]	Refs.
$Dry\ wood \rightarrow 0.2336\ Char(CH_\alpha O_\beta) + 0.0821\ CO + 0.1141\ H_2O + 0.1243\ CO_2 + 0.0057\ H_2 + 0.0165\ CH_4 + 0.0131\ C_2H_4 + 0.4106\ Tar$	$K^{pyr} = 2e^8 \cdot exp\left(-133100/_{R \cdot T_S}\right)$	[46, 47]
Char reactions	**Kinetics [m/s]**	**Refs.**
$Char(CH_\alpha O_\beta) + (1 - \eta/2 + \alpha/4 - \beta/2)O_2 \rightarrow \eta CO + (1 - \eta)CO_2 + \alpha/2 H_2O$	$K^{ox} = 5.7e^7 \cdot exp\left(-160400/_{R \cdot T_S}\right)$	[61]
$Char(CH_\alpha O_\beta) + CO_2 \rightarrow 2CO + (\alpha/4)H_2 + \beta H_2O$	$K^{g.1} = 3.42 \cdot T_S \cdot exp\left(-15600/_{T_S}\right)$	[62, 63]
$Char(CH_\alpha O_\beta) + (1 - \beta)H_2O \rightarrow CO + (1 + \alpha/2 - \beta)H_2$	$K^{g.2} = 5.7114 \cdot T_S \cdot exp\left(-15600/_{T_S}\right)$	[63]

Table 3
Homogeneous gas phase reactions.

Stoichiometry	Kinetics	Refs.
$C_{2.35}H_{3.97}O_{1.53}(tar) \rightarrow 0.3\ C_2H_4 + 0.25\ CH_4 + 0.89H_2 + 1.21\ CO + 0.16\ CO_2 + 0.13\ C(soot)$	$4.26e06\ exp\left(-\frac{1.08e08}{R \cdot T}\right)[C_{2.35}H_{3.97}O_{1.53}]$	[47,65]
$C_2H_4 + 2\ O_2 \rightarrow 2\ CO + 2\ H_2O$	$1.35e10\ exp\left(-\frac{1.2552e08}{R \cdot T}\right)[C2H4]^{0.1}[O_2]^{1.65}$	[66]
$CH_4 + O_2 \rightarrow CO + H_2 + H_2O$	$5.012e11\ exp\left(-\frac{2e08}{R \cdot T}\right)[CH4]^{0.7}[O_2]^{0.8}$	[32,66–68]
$CO + 0.5\ O_2 \rightarrow CO_2$	$2.03e11\ exp\left(-\frac{1.28e08}{R \cdot T}\right)[CO][O_2]^{0.5}[H_2O]^{0.5}$	[32]
$H_2 + 0.5\ O_2 \rightarrow H_2O$	$9.87e08\ exp\left(-\frac{3.1e07}{R \cdot T}\right)[H_2][O_2]$	[69,70]

equal to or greater than the evaporation temperature (100 °C). The fuel particles heat up and dry from the outside to the inside. The outer layer, once dry, can continue to increase its temperature above the evaporation temperature, while the interior of the particle is still drying. To model this effect in a thermally thin approach, part of the energy received by the particle is used to dry it (τ), while the remaining portion is utilized to heat it (1- τ) [58,59].

The dry wood is consumed due to the pyrolysis, which also generates char. The pyrolysis product composition is based on latest version of the detailed RAC scheme [46,47]. The scheme is applied for a typical soft-wood composition (44% cellulose, 26% hemicellulose, 30% lignin) [49] and fixed-bed conversion conditions, i.e. high charring and a slow heating rate (20 K/min) until a final temperature of 700 °C. The condensable species are grouped into the single tar specie and the solid products into the single char specie, which is described as $CH_\alpha O_\beta$, with α = 0.3934 and β = 0.0484 in molar basis [46,47,50].

The char consumption ratio is the sum of three reaction rates. These reactions are char oxidation with O_2 and gasification with CO_2 and H_2O. The diffusions of oxygen, carbon dioxide and water vapour are also considered as a rate limitation for each reaction. The CO/CO_2 ratio in char oxidation from Ref. [60] is employed; i.e. $CO/CO_2 = A\eta\ exp(-E\eta/T)$ [Aη = 12; Eη = 3300 K], being $\eta = CO/CO_2/(1 + CO/CO_2)$. The stoichiometry and kinetics of the pyrolysis and char reactions are shown in Table 2.

2.3. Gas phase

The conservation equations employed to solve the gas phase include continuity, momentum, energy, turbulence, chemical species and soot equations. Turbulence is modelled using the realizable k-ε model, which is widely utilized in simulations of biomass combustion systems [29,39]. The chosen gas flow formulation for the porous zone is the physical velocity, which takes into account the impact of section reduction on gas velocity. In addition, inertial and viscous resistance formulations, based on the physical properties of the particles, are incorporated to consider the effect of the porous zone on the gas flow [35]. The Finite-Rate/Eddy-Dissipation model is selected to model the turbulence-chemistry interaction [64].

The species considered in the gas phase include carbon monoxide (CO), carbon dioxide (CO_2), hydrogen (H_2), water vapour (H_2O), ethylene (C_2H_4), methane (CH_4), tars ($C_{2.35}H_{3.97}O_{1.53}$), oxygen (O_2) and nitrogen (N_2).

The stoichiometry of the tar cracking reaction is derived from the tar cracking scheme outlined in Ref. [47], and the kinetics are taken from Ref. [65]. These kinetics are utilized instead of those from Ref. [47] as they have demonstrated better suitability for this specific application, as observed in the simulation of a stove [32].

Table 3 presents the gas phase reaction scheme, including the kinetics for each reaction. The reactions considered include the tar cracking reaction, as well as the oxidations of ethylene, methane, carbon monoxide and hydrogen. The kinetics of the oxidations are taken from combustion schemes that are widely employed in biomass combustion cases. For the CO oxidation, a low temperature kinetic was selected, as it is deemed more suitable for the cases examined in this study [32]. The chosen soot model is the Moss-Brookes Model, considering the ethylene as the precursor specie and introducing the soot produced in the tar cracking as an additional soot source.

3. Methodology

This work presents a CFD study of a small-scale fixed-bed fuel-flexible biomass combustion plant, utilizing ANSYS-Fluent and the EBiTCoM fixed-bed model. Two cases were studied, varying the moisture content of the fuel. The numerical results are validated against experimental data [23].

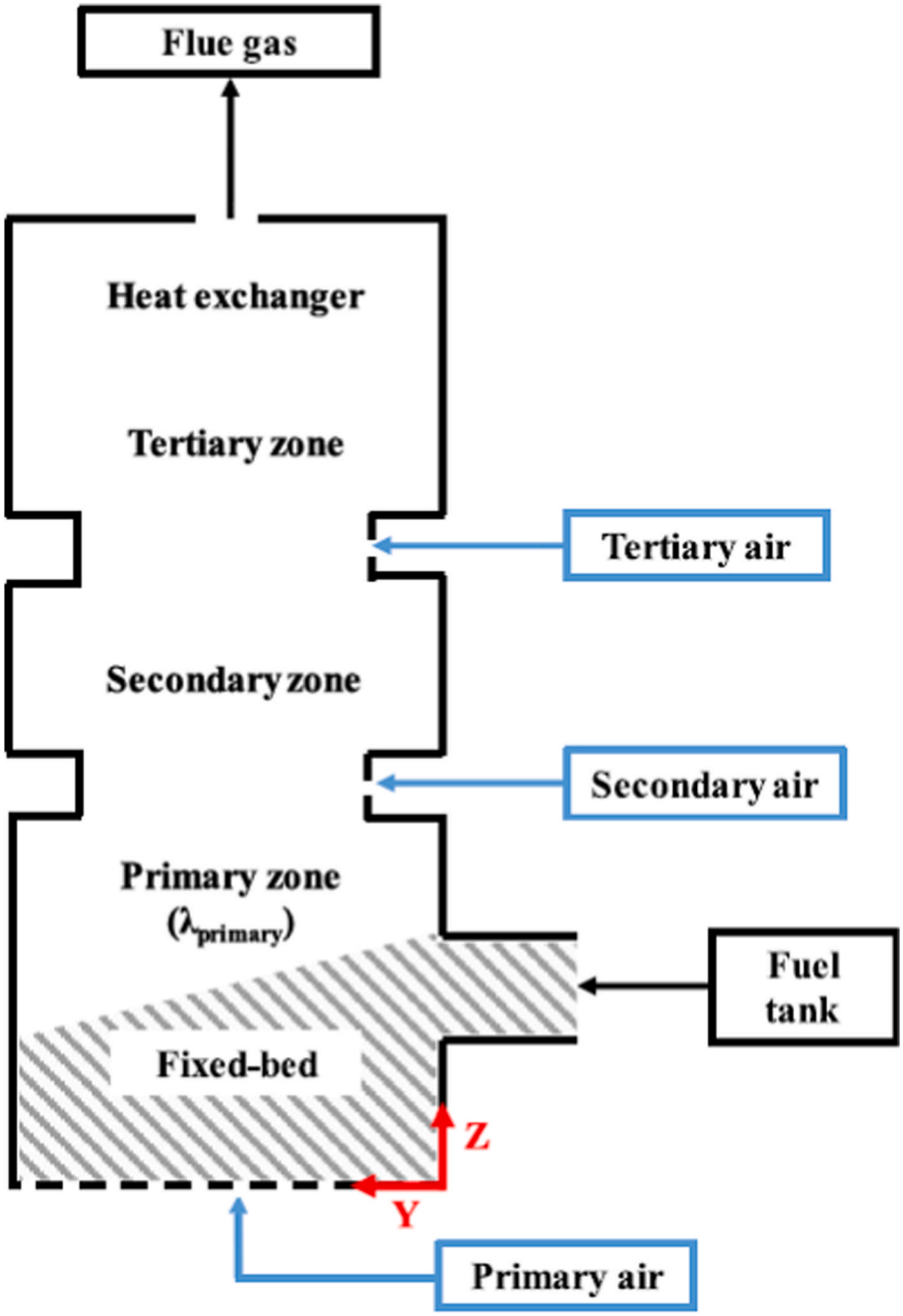

Fig. 2. Simplified schematic representation of the combustion plant. Adapted from Ref. [23].

3.1. System description and measurements

The combustion system is a 30 kW lab-scale plant that is designed to operate with a low oxygen concentration in the fixed-bed and with different biomass fuels [23].

The primary zone has a square cross-section and a height of 370 mm. The walls are made of fireclay bricks and externally water-cooled. At the bottom of this zone, a grate made of two steel parts with swivelling axes that allow retiring the ash once the operation cycle has ended, supports the solid fuel bed. The plant can operate continuously between 5 h and 10 h without ash removal depending on the ash mass fraction of the fuel. The primary air is introduced below the grate and fresh fuel is fed through an opening in one of the primary zone walls at 180 mm above the grate. Secondary air is introduced above the primary zone through 12 nozzles positioned around a circular section and oriented to create a swirling effect in the airflow.

Above the secondary air injection, there is the so-called secondary zone, and then there is the tertiary air injection, with the same configuration as the secondary air one, and its corresponding tertiary combustion zone. Following this section there is a 2-pass heat exchanger and the outlet. Fig. 2 shows a schematic view of the plant, indicating the location of each zone, the fuel inlet and the different air injection positions.

The experimental work [23] is focused on the determination of the different processes within the fixed-bed. Because of this, the data provided correspond to measurements taken within the primary zone. Measurements are carried out at four different levels inside the primary zone (Fig. 3a). Starting from the grate surface, the first set of in-bed temperature measurements is taken at a height of 5 cm, the second one at 11 cm and the third one at 17 cm. Above the solid fuel bed, at 32

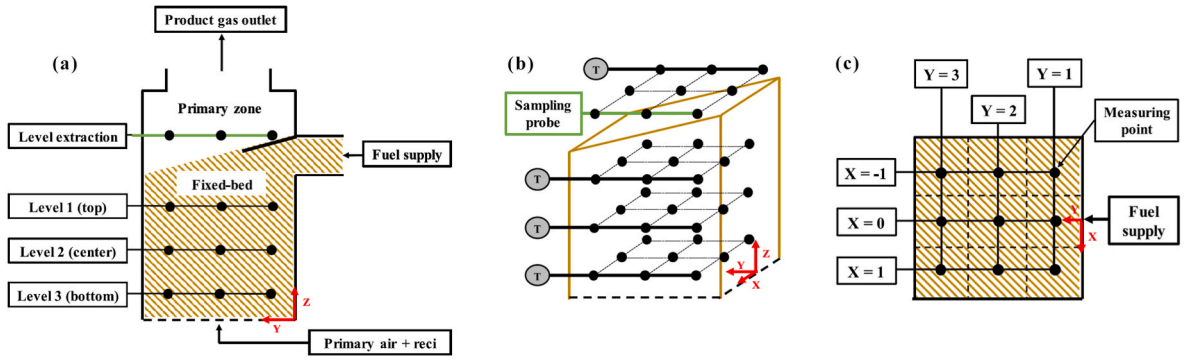

Fig. 3. Simplified schematic representation of the fixed-bed and primary zone including measurements positions in a vertical-cross section (a), oblique projection (b) and top view (c). Adapted from Ref. [23].

cm over the grate, another series of measurements, both of temperature and gas composition, is taken. Each set of measures consists in the data registered at nine different positions in the same horizontal plane (Fig. 3b). As can be seen in Fig. 3c, these nine positions are the result of dividing the cross-section in nine sectors. Each measurement is taken approximately at the centre of each division.

The temperature measurements are obtained using thermocouples at the four levels and the producer gas is extracted through a probe for its characterization at the extraction level. A sampling system is used to collect the tars and dry the extracted gas. Then a gas analyser is used to characterize the dry tar-free gas composition. The experimental data [23] includes the average temperature for each level, the volume fraction of CO, CO_2, CH_4 and H_2 in the dry gas for the nine extraction points and the mass of tar collected per normal cubic meter of analysed gas for the same points.

3.2. Fuel and operating conditions

The design of the plant allows the use of different types of biomass fuels. In the experimental work, several cases using wood chips with different moisture contents and miscanthus pellets are presented, including flue gas recirculation in some cases [23]. In this work, two different cases using P16S wood chips with 8% (w8 WOR) and 30% (w30 WOR) moisture content without the use of flue gas recirculation are studied. These two cases were selected to study the impact of fuel moisture content on thermal conversion processes and emissions. The properties of the fuels are presented in Table 4.

The operating conditions for the studied cases are shown in Table 5. The two chosen cases correspond to the experimental test where the two mentioned fuels are used, and no flue gas recirculation is applied.

3.3. Discretization and boundary conditions

The system has to be discretized into control volumes in order to apply the CFD methodology. The discretized domain includes mainly the gas zones. These are the primary, secondary and tertiary air plenums, the primary, secondary and tertiary combustion zones, and the heat exchange zone. Also, the solid parts that are located between these zones, as the grate, are also meshed. Neither the surroundings nor the solid of the walls that enclose the gas zones have been meshed. In these cases, different boundary conditions have been applied to these walls.

The walls of the primary zone are made of fire-bricks while the other walls are made of steel. In the secondary and tertiary zones, where high temperatures are expected, there is a layer of vermiculite over the steel walls to protect them. The thermal properties of each material are applied to each solid part, if it has been meshed, and to the boundary walls, including their thickness. Regarding the heat transfer from the boundary walls to the exterior, convection is considered. For the primary, secondary, tertiary and heat exchange zones, which are water-cooled, convection to water conditions are applied. For the other walls, convection to still air is considered [36,39]. Also, an emissivity value of 0.8 is applied to the internal walls to take into account the influence of the fouling layer in the radiation heat transfer [39].

Mass flow inlet conditions are applied to the primary, secondary and tertiary air inlets. The primary air flow and fuel feeding rates are shown in Table 5. The fresh fuel is fed continuously using the saturation method presented in previous work [39].

Polyhedral cells have been chosen as discretization elements. This type of cells allow to reduce the number of elements needed to discretize the domain in comparison with tetrahedral cells and result in better performances of the bed physics algorithms [56,57]. The mesh is more refined near the walls and where higher gradients are expected, as in the bed region or in the air injection nozzles. After conducting mesh dependence tests, a mesh composed of around one million cells was chosen. One of the assumptions of this Eulerian model is to consider the bed as a dispersed porous medium with volume-averaged properties within each cell. For this assumption to be correct, each cell must be a porous medium composed of several fuel particles. Therefore, the size of the cells has to be larger than the size of the fuel particles. The mesh in the bed zone is more refined towards the walls and about 0.5 cm above the grate, due to the discretization of the grate primary air holes. Disregarding these smaller cells, the average cell size in the bed is around 0.7 cm3, with cells up to 1.85 cm3 in volume. This volume is greater

Table 4
Fuels characterization [23].

Parameter	Unit	Wood chips (w8)	Wood chips (w30)
H_2O	Mass fraction[a]	8.0%	30.7%
C	Mass fraction[b]	50.7%	50.7%
H	Mass fraction[b]	6.0%	6.0%
O	Mass fraction[b]	42.5%	42.5%
N	Mass fraction[b]	0.1%	0.1%
Ash	Mass fraction[b]	0.7%	0.7%
GCV	MJ/kg[b]	20.4	20.4
NCV	MJ/kg[a]	17.4	12.4

[a] Wet basis, as received.
[b] Dry basis with ash.

Table 5
Operating conditions of the simulated experimental test runs [23].

Parameter	Unit	w8 WOR	w30 WOR
Fuel power	kW	32.7	28.7
Fuel mass flow	kg/h	6.8	8.3
$\lambda_{primary}$	–	0.20	0.21
Primary air mass flow	kg/h	7.5	7.4
Fixed bed height	M	0.25	0.25
Primary air temperature	°C	20.0	22.7

than the average volume of fuel particles, so it is correct to consider that several particles reside in each cell. In smaller cells where this premise is not true, the values shall be understood as representative of an averaged volume of a specific region of the bed and not of the particles within the cell [37].

4. Results and discussion

4.1. Pseudo-steady state conditions

A transient simulation was carried out for each case. The simulation starts with a fresh fuel bed that is ignited applying a radiation source to the bed. Once the fuel has dried out and starts to burn, this heat source is disconnected and fresh fuel is fed, aiming for a self-sustaining combustion. Variables such as flue gas temperature, heat of reaction, oxygen excess or solid fuel mass are continuously monitored to check the evolution of the simulation, which is carried out until a pseudo-steady state with stable combustion is reached. Combustion of solid biomass presents a pulsating behaviour [71]. Therefore, some of the monitored variables will describe an oscillation. The solution is considered converged when the monitored variables tend to a stable value or to oscillate periodically with a constant mean value, in what can be considered as a pseudo-stationary state.

In the experimental work, the operating point of each test run is defined by two parameters: fuel mass flow and primary air mass flow (or primary lambda), which result, for both cases, in a solid fuel bed height of 0.25 m above the grate surface (Table 5).

In order to have a constant bed height, it is necessary that the thermal conversion ratio of the fuel is equal to the fuel feeding ratio. In other words, the fuel has to be consumed at the same rate at which it is introduced. The primary air flow is the parameter that controls the thermal conversion ratio of the solid fuel. A higher primary lambda results in faster fuel consumption rates and lower primary air ratios lead to longer fuel residence time before it is totally consumed.

For the simulations, it has been decided to set the same fuel mass flow rates as in the experimental tests, keeping them constant, and search for the primary air flow rate that results in a constant bed height equal to that reported in the experimental work. In both simulated cases, the initial operating conditions chosen for the fuel mass flow and primary air mass flow were the same as for the experimental tests (Table 5).

During the calculations it has been seen that, for the initial conditions, the solid fuel bed height increases continuously and exceeds the 0.25 m height because the primary air flow rate is not sufficient to make the fuel thermal conversion rate equal the feed rate. In order to find the operating conditions to keep a constant solid fuel bed volume, several calculations, increasing progressively the primary air fuel ratio, were carried out. It has been found that primary air flows of 8.28 kg/h and 7.62 kg/h for the w8 WOR and w30 WOR cases respectively, result in constant solid fuel bed volumes with an approximate height of 0.25 m. With these conditions, the volume of wood and char in the bed are practically constant with only a very slow bed height increase due to the accumulation of inert ash in the lower part of the bed, above the grate. The final operating points correspond to a primary air lambda of 0.22 for both fuels. This obtained value in the model that leads to bed height of 0.25 m is very close to the experimental values for primary air lambda of 0.20 and 0.21, which shows the suitability of the employed model to predict with a good accuracy the required primary air lambda to obtain a certain bed height. For both cases, the slight increase of primary air ratio in comparison to the experiments has been compensated by decreasing the secondary air ratio to maintain the global lambda at a constant value of 1.5.

The calculation is run until all the monitored variables are stable, or describing periodically oscillations around a stable mean value, which means that a pseudo-stationary state has been reached and convergence has been achieved. Once the pseudo-stationary state has been reached, the temperature and species monitors were recorded for 5.000 s of flow-time, to obtain time-averaged values. The graphs showing comparisons between numerical and experimental data present time-averaged values

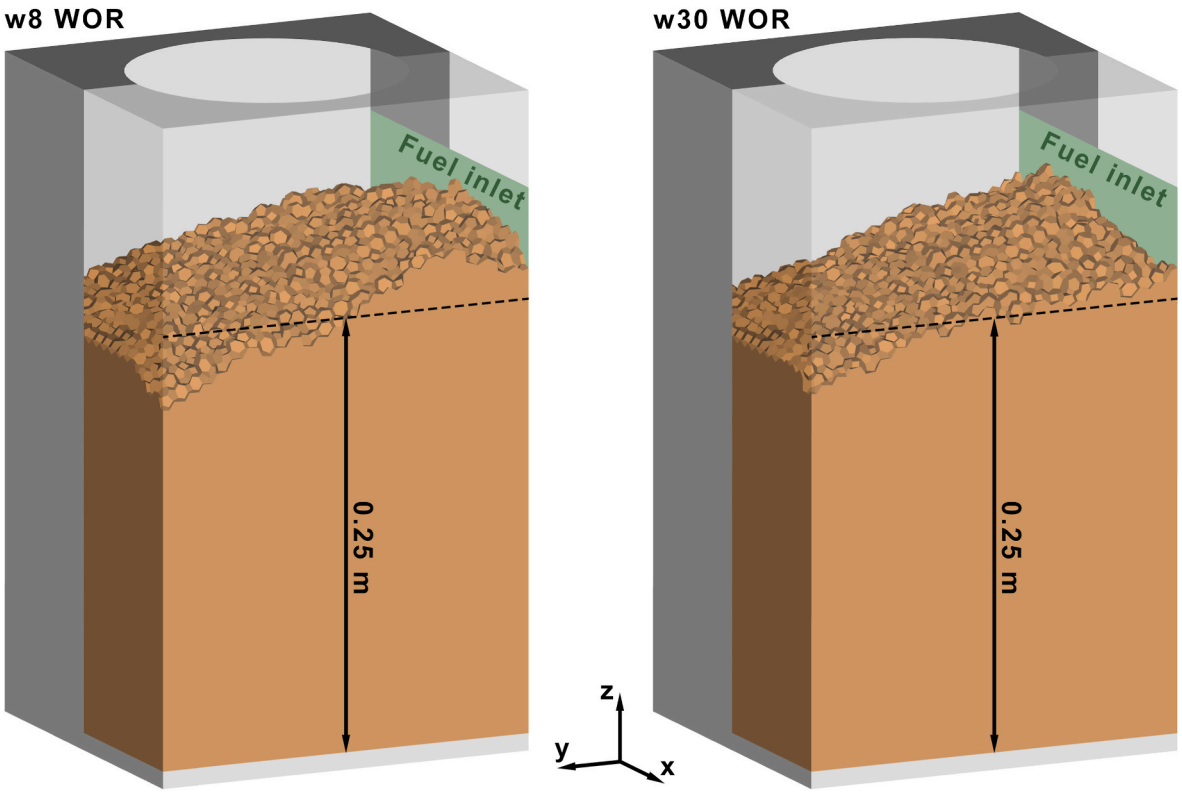

Fig. 4. Bed shape and height contours. In brown, cells in which solid fuel is present.

for both data series. However, the CFD contours correspond to a specific moment (time-step) within the chosen interval. Since there is no major change in the state of the solid fuel bed once the pseudo-steady state has been reached, the chosen time step can be considered representative of the whole interval.

As can be seen in Fig. 4, the solid fuel bed has a similar height and shape for both cases. The beds are higher on the right side, where the fuel inlet is located, with a downward slope towards the opposite wall. The average height of the beds is around 0.25 m for both cases, which was the target height. The bed shape is in line with the experimental results as can be seen in the schematic drawings presented in Figs. 2 and 3.

4.2. Comparison to experimental product gas composition and temperatures

The numerical results obtained will be compared against the experimental data [23]. The gas composition and temperature above the solid fuel bed will be analysed. In addition, the temperature distribution inside the solid fuel bed is studied. The experimental data correspond to average values with their corresponding standard deviations.

4.2.1. Product gas composition

The gas measurements presented are the volume fractions of carbon monoxide, carbon dioxide, methane and hydrogen, all of them related to dry product gas (without water vapour and condensable tars) at standard conditions. Figs. 5 and 6 present the comparison of the spatial distribution of species at the extraction level between the CFD results and the experimental data for both studied cases. The experimental data presented are the time-averaged volume fraction, in tar-free dry gas basis, for each specie, with its standard deviation, at each of the nine coordinates. The tar concentration is measured as mass of condensed tar per volume of tar-free dry gas analysed. The numerical results are presented as three-dimensional surfaces representing the concentration of each specie at the extraction level. For all cases, the x and y axes represent the horizontal dimensions of the system and the z axis the concentration value of each specie.

In Fig. 5 it can be seen how the CO experimental measurements have a fairly homogeneous value for the 9 points in both cases. The measurements vary slightly, being higher at the points closest to the fuel inlet wall (Y = 1) and decreasing towards the opposite wall. The numerical results are even more homogeneous than the experimental results, with a slight tendency for the maximum values to be on the wall opposite the inlet (Y = 3). The CO_2 distribution for the w8 WOR case presents the maximum values at Y = 1 points, decreasing to the middle of the grate and with a slight increase towards the end. The model also predicts the maximum concentration at the inlet side but with a continuous decrease in concentration towards the opposite wall. For the w30 WOR case, the CO_2 measurements present a homogeneous distribution of CO_2 at the extraction level both in the experimental and numerical case.

The CFD distribution of CH_4, as can be seen in Fig. 6, resembles the one of CO_2 but with lower concentration, for both cases, showing a good agreement between experimental and numerical data. As for the H_2 distribution, for the w8 WOR case, the model results show an overestimation of the hydrogen volume fraction at the points closest to the fuel inlet. This can be attributed to the absence of air infiltration through the supply system, which is not considered in the numerical case. This air would oxidise the hydrogen in the region near the fuel inlet decreasing its concentration. Despite this, the decreasing trend towards

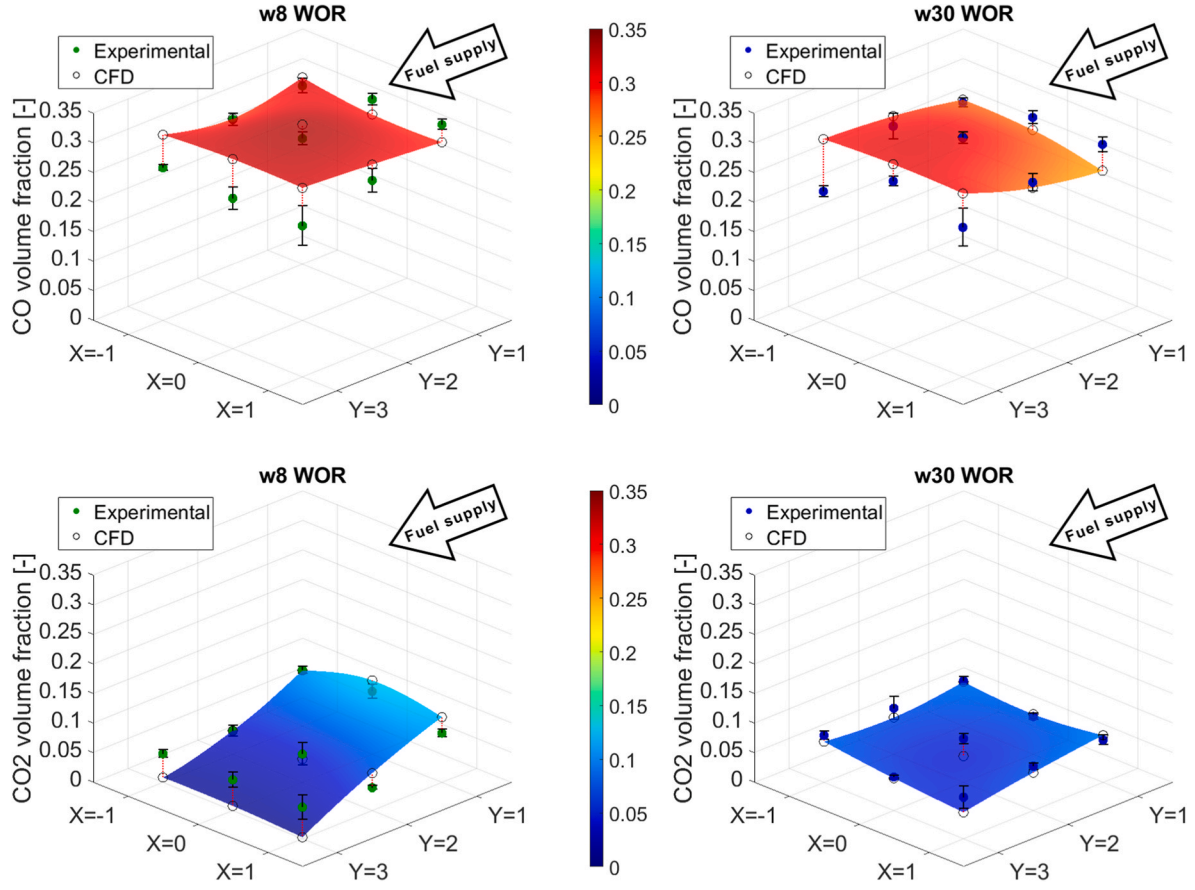

Fig. 5. Comparison of CFD and experimental [23] data of the spatial distributions of CO (top) and CO_2 (bottom) concentrations at the gas extraction level for the positions depicted in Fig. 3c.

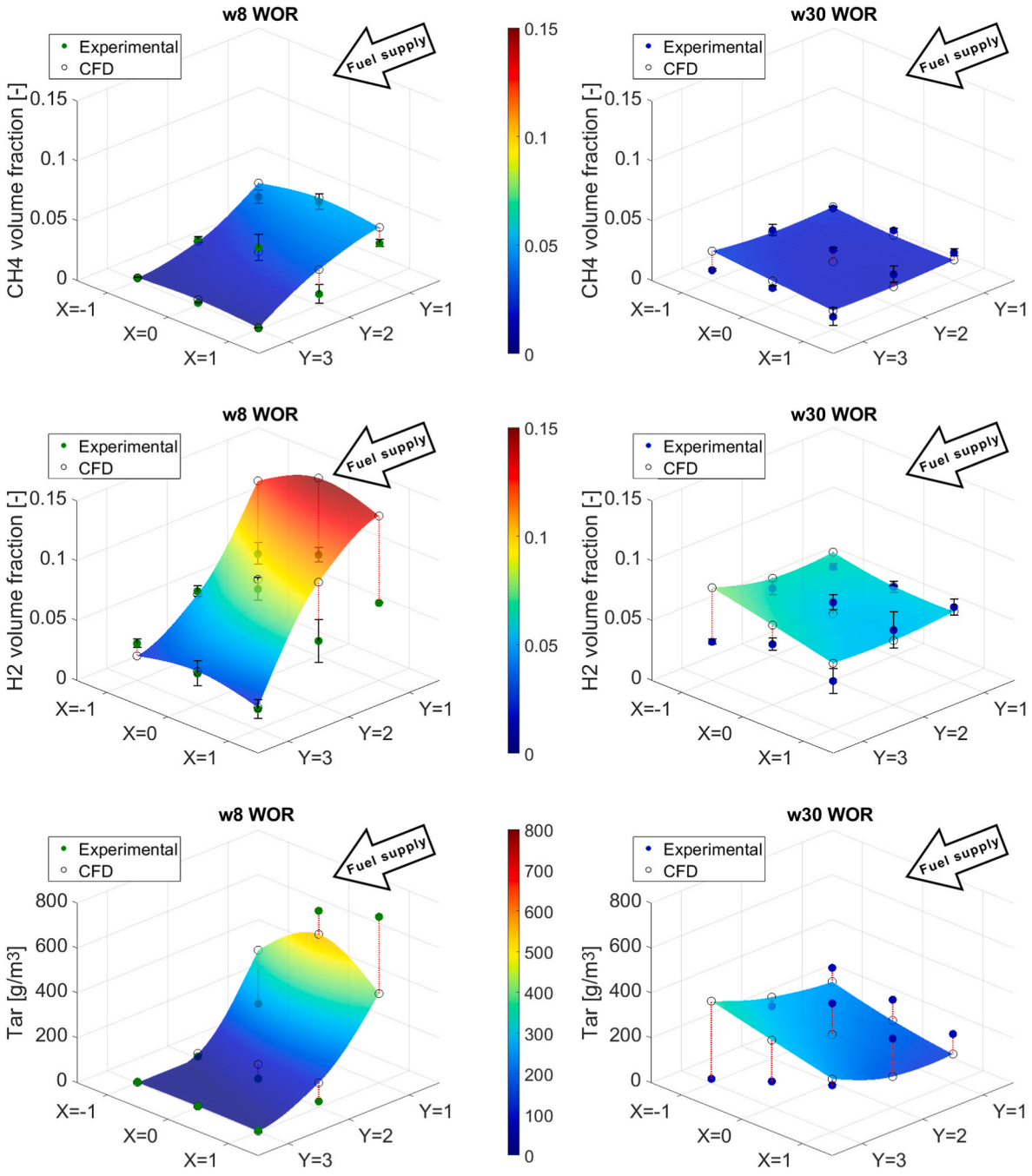

Fig. 6. Comparison of CFD and experimental [23] data of the spatial distributions of CH_4 (top), H_2 (middle) and tars (bottom) concentrations at the gas extraction level for the positions depicted in Fig. 3c.

the end of the grate and the values at these points are predicted correctly. The w30 WOR case measurements show a homogeneous release of H_2 all over the surface. The numerical values fit reasonably well this distribution but with a slight overestimation of the concentration towards the (−1, 3) corner.

The spatial distribution of condensable tars (bottom of Fig. 6) is similar to that of H_2 for both cases. In the 8% moisture content case, the higher tar concentrations are detected at the points closest to the inlet. At these points (Y = 1) the model predicts a symmetrical release, with the maximum value at the centre and similar values at the right and left points. However, the experimental extractions show a not uniform distribution of tars, with a higher release of tars towards the left side looking from the inlet to the inside of the system (X = 1). Using an auger conveyor to supply the fuel causes the majority of the fuel to enter to the right side (X = -1), which makes the drying the dominating process in this zone. Once dried, the fuel crumbles to the position (1, 1) where its pyrolysis takes place, causing this high release of tars towards that side [23]. However, the saturation feed method introduces the fresh fuel through the designated inlet boundary by pushing it homogeneously into the system in the y-axis direction. For this reason, in contrast to experimental measurements, the simulation gives a more symmetric tar distribution around the fuel inlet. Towards the centre and the opposite side, the tar concentration decreases abruptly in both the experimental case and the numerical simulation. As for the 30% fuel moisture case, the spatial tar distribution is much more homogeneous that in the other case and no clear trend is discernible. The comparison between experimental and numerical data shows the most notable discrepancy in the (−1, 3) corner, where the model has predicted the maximum tar

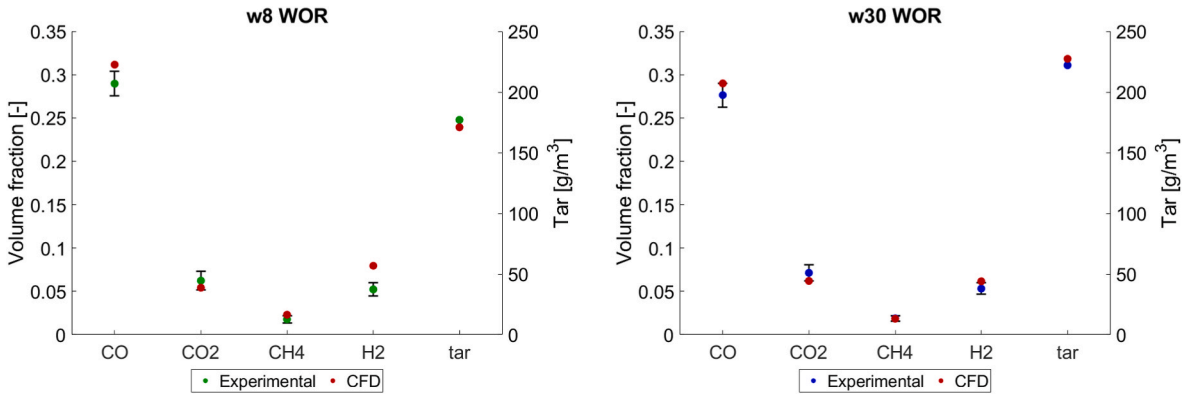

Fig. 7. Comparison of the CFD and experimental [23] surface average gas composition at the extraction level.

concentration in contrast to the minimum value measured in the experimental work.

The analysis of the spatial distribution of species shows that the moisture content of the fuel has a strong influence on the zones where pyrolysis volatiles are released. The w30 WOR case shows a more homogeneous distribution of species over the whole bed surface than the 8% case, whose distributions show high gradients from the fuel inlet to the opposite wall. Overall, the trends identified experimentally are reasonably well represented, with some minor discrepancies, by the numerical simulation.

To check whether the new pyrolysis mechanism correctly predicts the biomass conversion into volatile species, in Fig. 7 the experimental and numerical surface average concentrations of each compound at the extraction level are compared. In both cases, the CO yield predicted is slightly higher than the experimental measurements, with an 8% error for the w8 WOR case and 5% for the w30 case. On the other hand, CO_2 is slightly underestimated in both cases but with values very close to the experimental. The CH_4 is predicted almost exactly in both cases but the H_2 is overestimated, especially for the w8 WOR case, as had already been detected in the analysis of the spatial distribution of H_2 (Fig. 6). The tar concentration, which is measured in grams per meter cubic of tar-free dry gas extracted, is close to the numerical results in both cases, with an underestimation of 3% for the w8 WOR case and an overestimation of 2% for the w30 WOR case.

It has been proven that, in both cases, the model can predict with a good accuracy the product gas composition. At the extraction level, a low CO_2 concentration and a high CO and tar concentrations have been detected. This is a direct result of low primary lambda conditions, which make the system work as a gasifier in the primary zone.

4.2.2. Temperatures

In Fig. 8, the temperature distribution in the primary zone for the two cases studied is shown. The experimental points show the average of the temperature measured at the nine measurement points at each level, three inside the fuel bed and one at the gas extraction level. The numerical data present the continuous distribution, along the vertical axis, of surface average temperature from the grate to the extraction height. In both cases, it can be seen that the maximum temperature, around 1100 °C, is achieved around 2–3 cm above the grate. The position of this zone is conditioned by the height of the layer of ash accumulated in the lower part of the bed. The values calculated for the w8 WOR case fit quite well with the values measured inside the bed. As for the gas temperature at the extraction level, a value higher than the experimentally measured one has been predicted. On the other hand, for the w30 WOR case, the largest deviation between the CFD and experimental results is observed in the measurement closest to the grate, where the experimental value is slightly higher than the calculated value.

It can be seen that, in both cases, there is a high temperature gradient inside the solid fuel bed in the vertical direction. Because of this, any small displacement of the thermocouples could result in a significant variation of the temperature measured. This is also reflected in the high values of the standard deviations of the experimental measurements. Taking this into account, it can be considered that the numerical model predicts the solid fuel bed temperatures with good accuracy. The model correctly predicts that for the w30 WOR case temperatures are significantly lower at the top of the primary zone than for the w8 WOR case, while the temperatures close to the grate are similar. The most notable deviation occurs in the gas phase temperature measurement for the w8 WOR case. In this case, from the bed surface (0.25 m), a temperature slightly below 700 °C, and almost constant, is predicted along the vertical axis. For the case of fuel with a 30% moisture content, the minimum temperature is reached around the surface of the bed. From this point on, there is a progressive increase in temperature, reaching 400 °C at the gas extraction height.

The temperature difference in the zone between the bed surface and the gas extraction is the main cause of the tar concentration difference shown in Fig. 7. The tar cracking reaction rate is temperature dependent and for temperatures below 500 °C the reaction rate is negligible [50]. Because of this, in the w30 WOR case, tar cracking does not occur below the gas extraction zone, while in the w8 WOR case it does although to a low extent, resulting in a tar concentration around 50 g per cubic meter of dry gas lower than in the w30 WOR case.

4.3. Conversion zones and discussion of results

To analyse in depth the model behaviour and the differences between both cases, the contours of the solid fuel bed temperature and components will be studied. Fig. 9 shows the temperature contours of the solid fuel bed, including a cross-section to analyse the temperature distribution inside the bed. There is a clear influence of the moisture content of the fuel on the bed temperatures as already seen in the data shown in Fig. 8. In both cases, the maximum temperature zones are close to 1200 °C and are located above the accumulated ash layer, where the primary air passing through the grate meets the char. This air flow produces the oxidation of char, which is the most exothermic of the reactions taking place inside the bed. From this area, the temperature decreases progressively towards the upper part of the bed. This cooling is faster for the w30 WOR case, as the temperature of the fuel at the upper part of the bed is lower due to drying taking place to a higher extent, resulting in a higher thermal gradient.

In the full volume contour of the w30 WOR case, it can be seen that, towards the wall opposite the fuel inlet, the bed temperature distribution is not symmetrical. There is a higher accumulation of colder fuel towards the right-hand corner, looking from the inlet. Taking into account that the system is symmetrical with respect to the y-z plane, the fuel is fed around the centre of the fuel inlet and that the primary air is distributed homogeneously across the horizontal section of the bed, it can be inferred that this asymmetry can be attributed to a computational

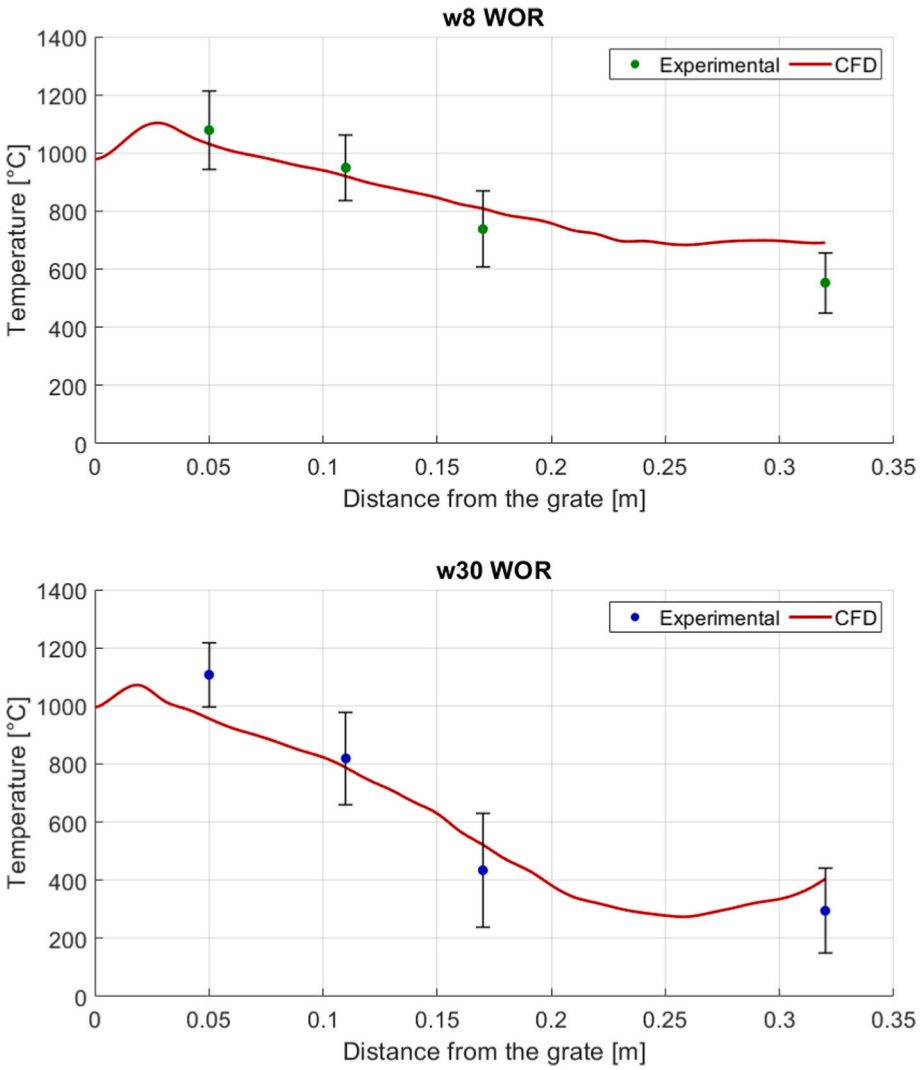

Fig. 8. Comparison of the CFD and experimental [23] temperature distribution in the primary zone along the vertical axis.

reason. The solid bed movements algorithms are based on vector operations over the geometric structure of the mesh [56,57]. The polyhedral mesh used in these cases is not structured which means that the mesh is not symmetrical. In addition, the bed physics algorithms work with cell loops to move the solid fuel from one computational cell to another. The loop of cells is controlled by the CFD code and is always performed in the same cell order. This, combined with the mesh being not structured, results in preferential paths for solid fuel movements, especially in the case of the fresh fuel entering the system, leading to a higher accumulation of colder fuel on the bed surface towards the corner mentioned above. This zone corresponds to the measurement point (−1, 3), where the largest deviations were found for the case w30 WOR. At this point, the predicted hydrogen and tar fractions showed a larger deviation than in the other 8 points. These overestimates are a direct consequence of the preferential paths that cause the fresh fuel to reach this zone of the bed, where it is pyrolyzed.

The model also allows to visualize the solid fuel bed composition, as seen in Fig. 10. The contours of moisture, wood and char content show the different stages of the thermal conversion of the fuel. The influence of the moisture content on the thermal conversion of the fuel can be clearly seen by comparing the contours of both cases. For the w8 WOR case, due to the high temperature in the zone (around 700 °C), the fed fuel dries very fast, which causes the wood to pyrolyze very close to the fuel inlet. This results in low wood accumulation and a very localised release of water vapour and pyrolysis volatiles, in front of the fuel inlet, as have been seen in the analysis of the species spatial distribution.

On the other hand, for the 30% moisture case, the fuel needs more time to dry. As it can be seen in the moisture contours, both the moisture content and the accumulation of wet fuel are higher than in the w8 WOR case. The wet fuel even reaches the rear wall, accumulating towards the corner, with the consequent accumulation of wood in this zone, as can be seen in the wood contour. As already discussed, this tendency of the fresh fuel to move to this zone is the cause of the major discrepancies, between the experimental and the CFD, detected at the (−1, 3) measurement point. Apart from this, the w30 WOR case show that there is a layer of wood over the entire surface of the bed, which results in a homogeneous pyrolysis species distribution, unlike the 8% moisture case, where there is a localised wood pyrolysis front near the fuel inlet. These results are in accordance with the species spatial distribution analysis, showing a correlation between the drying and pyrolysis fronts and the species detected in each measurement point.

Finally, we can see that in both cases the bed is mainly composed of char, with a thin layer of compacted ash in the lower part. This high amount of char is a direct consequence of the low primary air conditions used, which makes the system work like a gasifier, with a small fraction of the char being consumed by oxidation and most of it by gasification, which favours a higher char accumulation. For this reason, the major specie predicted above the bed is CO, which is the main product of gasification, and is homogeneously distributed since the char layer occupies the entire horizontal section of the bed.

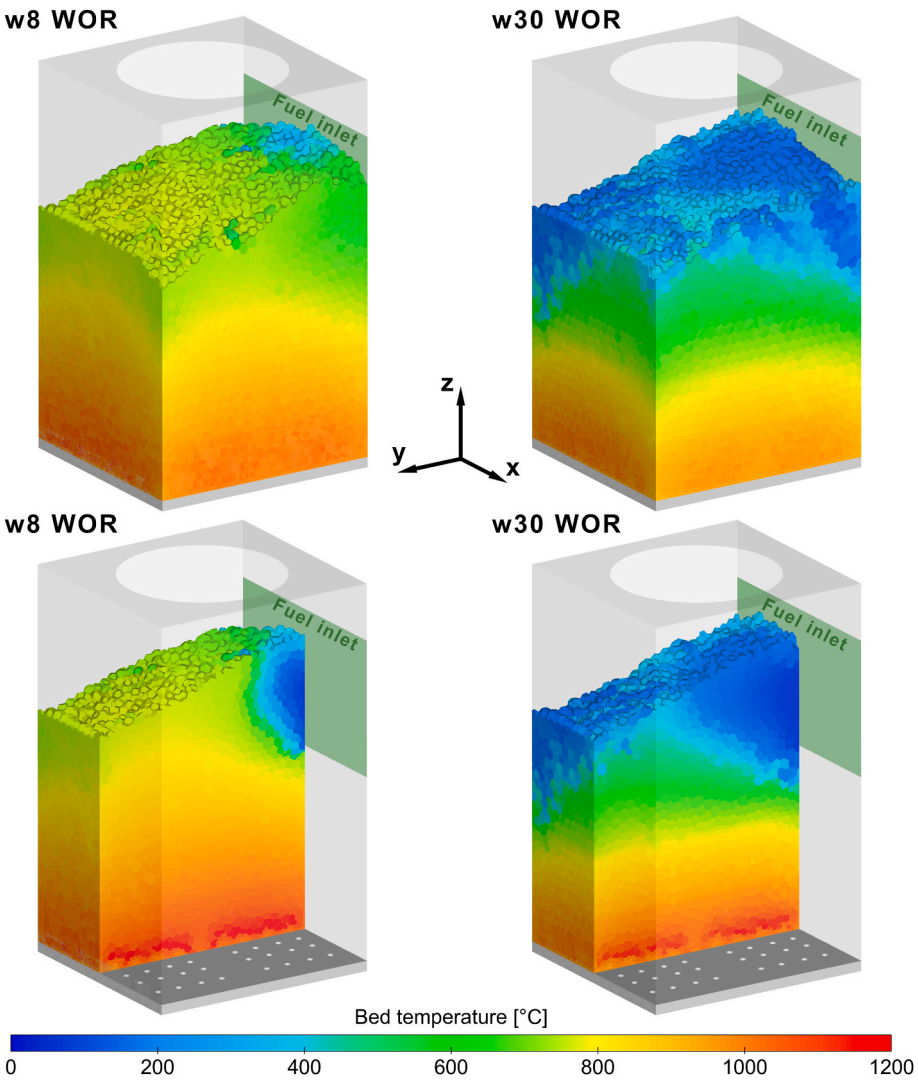

Fig. 9. Temperature contours of the solid fuel bed. Full volume (top) and mid-plane (x = 0) cross-section (bottom).

The results shown in this work represent a significant advance in modelling novel combustion technologies with a low primary air ratio in the fuel bed. The current experimental results were already modelled with a one-dimensional bed conversion model [50], showing a good agreement for the surface average product gas composition at extraction level and for bed temperatures and conversion zones along the height of the reactor. However, this previous work had several limitations, i.e. the spatial distribution of the release of species could not be predicted, the bed height had to be fixed for the simulations, and thermal boundary conditions at the grate and top of the bed had to be pre-defined based on assumptions. These limitations are overcome in the current work, which has a higher and more detailed predictability and therefore represents a significant advance in the understanding of the conversion processes in novel combustion technologies with a low primary air ratio in the fuel bed.

5. Conclusions

An Eulerian Biomass Thermal Conversion Model was modified to include a biomass reaction mechanism obtained from the application of a detailed pyrolysis scheme (RAC) for softwood. Its implementation in a detailed three-dimensional CFD model allowed for the assessment of its accuracy in predicting the spatial distribution of conversion zones within the fixed bed, as well as temperatures and released volatiles. For this purpose, a small-scale biomass combustion system with low primary air ratio was simulated. Two cases were examined, each using fuels with different moisture contents (8% and 30% by mass). The obtained results were validated against experimental data.

The model was able to correctly predict the solid fuel bed height and shape. Temperature and species distribution are also predicted with reasonably good accuracy, correctly characterising the thermal conversion processes for both fuels. The moisture content of the fuel has a significant impact on the pyrolysis front size and location. The fuel with higher moisture content leads to a more homogeneous distribution of volatiles over the bed surface. Nonetheless, the average composition of the dry gas is very similar for both cases. The model shows a slight overestimation of the CO concentration by 8% and 5% for each respective case. On the other hand, the CO_2 content in the producer gas is slightly underestimated. The results for the CH_4 and H_2 content closely match the experimental values, except for the H_2 concentration in the 8% moisture content case. In this case, higher concentrations of H_2 are observed towards the fuel inlet, which may be attributed to no considering air infiltrations.

In both cases, the bottom part of the solid fuel bed consists of a thin layer of ash and a thick layer of char. The maximum temperatures, approximately 1100 °C, are recorded at the bottom of the char layer for both cases. From that point, the temperatures gradually decrease towards the bed surface. While for the 8% moisture case the minimum

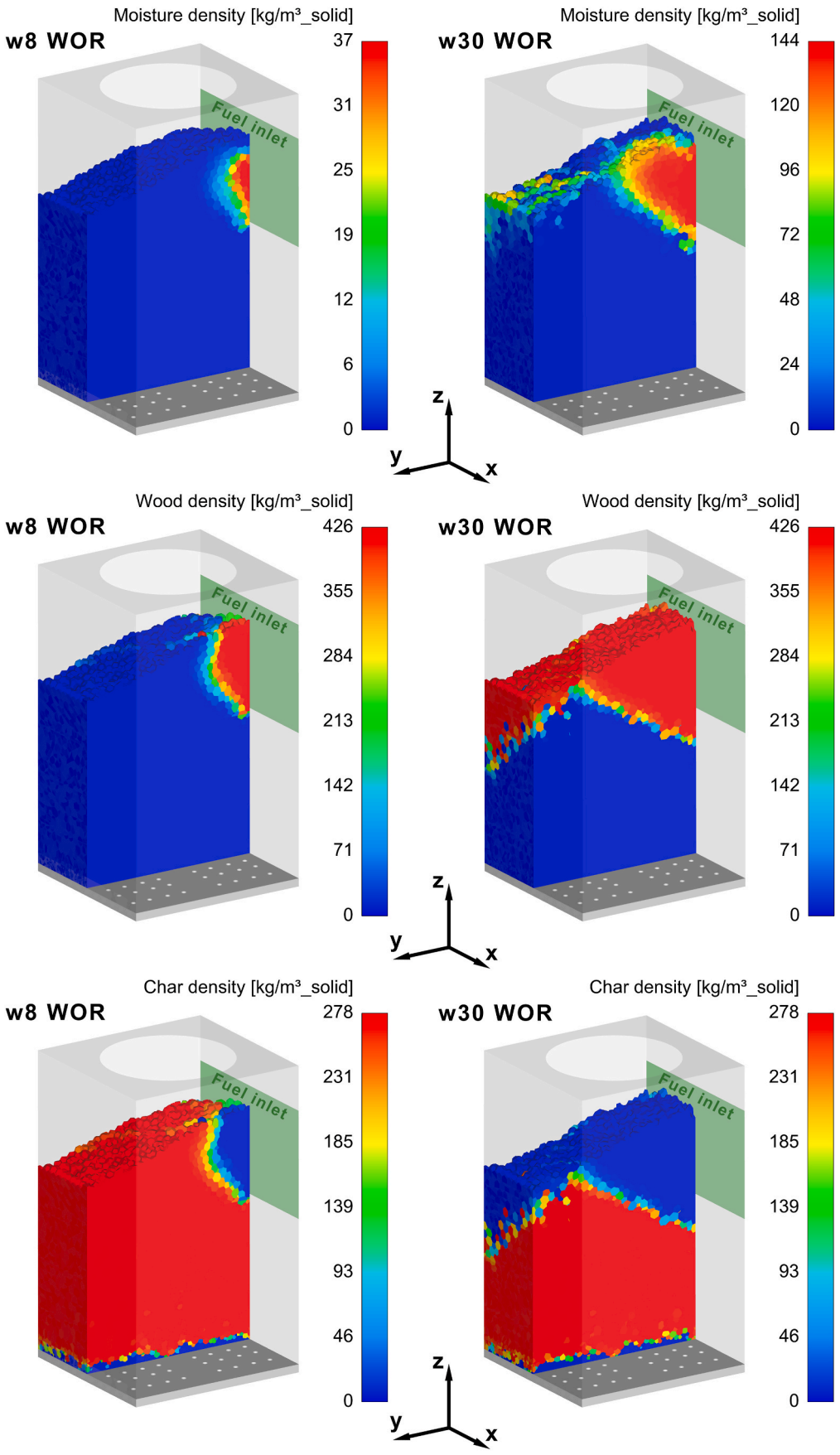

Fig. 10. Solid fuel bed components densities contours at the mid-plane (x = 0) cross-section.

temperature predicted is around 700 °C above the solid fuel bed, for the 30% case there is a higher temperature decrease, going down to 300 °C in the gas zone. The lower temperatures above the bed impede the tar cracking reaction, leading to a 25% higher tar content in the producer gas in the case with 30% moisture content fuel.

It has been demonstrated that three-dimensional modelling provides valuable information about the thermal conversion of biomass in combustion systems. The developed model is a valuable tool for simulating biomass combustion systems with beds consisting of numerous fuel particles, allowing for calculations of long boiler operating time with affordable computational requirements. As future work, modelling the formation of pollutant emissions such as NOx or PM can be considered, along with studying emission reduction methods like flue gas recirculation.

CRediT authorship contribution statement

César Álvarez-Bermúdez: Conceptualization, Data curation, Formal analysis, Investigation, Methodology, Software, Validation, Visualization, Writing – original draft. **Andrés Anca-Couce:** Conceptualization, Investigation, Methodology, Validation, Writing – review & editing. **Sergio Chapela:** Methodology, Software, Validation, Writing – review & editing. **Robert Scharler:** Supervision, Writing – review & editing. **Markus Buchmayr:** Validation, Writing – review & editing. **Miguel Ángel Gómez:** Methodology, Software, Supervision, Validation, Writing – review & editing. **Jacobo Porteiro:** Funding acquisition, Project administration, Resources, Supervision, Writing – review & editing.

Declaration of competing interest

The authors declare the following financial interests/personal relationships which may be considered as potential competing interests: Cesar Alvarez-Bermudez reports financial support was provided by Spain Ministry of Science and Innovation.

Acknowledgments

This research was funded by the project PID2021-126569OB-I00 of the Ministry of Science and Innovation (Spain). The work of César Álvarez-Bermúdez has been supported by the grant PRE2019-090110 of the Ministry of Science and Innovation (Spain). Funding for open access charge: Universidade de Vigo/CISUG.

Nomenclature

Acronyms

CFD	Computational Fluid Dynamics
GCV	Gross calorific value
NCV	Net calorific value
PM	Particulate matter
RAC	Ranzi-Anca-Couce
UDF	User Defined Function
UDS	User Defined Scalar

Latin symbols

Av	area-volume ratio
CP	specific heat [J/kg·K]
K	reaction constant [1/s] or [m/s]
LH	latent heat [J/kg]
Mi	molecular weight of the i component [kg/kmol]
R	ideal gas constant [J/mol·K]
T	Temperature [K]
t	Time[s]

Greek symbols

λ	air-fuel equivalence ratio [−]
ρ	density [kg/m^3]
τ	fraction of heat received by the particle employed in drying [−]
$\dot{\omega}_i^{'''}$	consumption or generation rate of the *i* component [kg/m^3·s]

Subscripts

C	consumption
char	char
evap	evaporation
G	generation
glob	global
i	wood components (moisture, dry wood, char and ash)
moisture	moisture
p	particle
primary	primary air
s	solid
wood	dry wood

Superscripts

g,1	char gasification with CO_2
g,2	char gasification with H_2O
ox	char oxidation
pyr	pyrolysis

References

[1] IEA, *Renewables*, Analysis and Forecast to 2025, International Energy Agency, 2020, 2020.

[2] J. Sánchez, M.D. Curt, N. Robert, J. Fernández, Biomass Resources," *the Role of Bioenergy in the Bioeconomy*, Elsevier, 2019, pp. 25–111.

[3] J. Islas, F. Manzini, O. Masera, V. Vargas, Solid Biomass to Heat and Power," *the Role of Bioenergy in the Bioeconomy*, Elsevier, 2019, pp. 145–177.

[4] A.S. Tomlin, Air quality and climate impacts of biomass use as an energy source: a review, Energy.mathsemicolon Fuels 35 (Jul) (2021) 14213–14240.

[5] S. Chapela, J. Porteiro, M.A. Gómez, D. Patiño, J.L. Miguez, Comprehensive CFD modeling of the ash deposition in a biomass packed bed burner, Fuel 234 (Dec. 2018) 1099–1122.

[6] S. Chapela, J. Porteiro, M. Garabatos, D. Patiño, M.A. Gómez, J.L. Miguez, CFD study of fouling phenomena in small-scale biomass boilers: experimental validation with two different boilers, Renew. Energy 140 (Sep. 2019) 552–562.

[7] Y. Cai, K. Tay, Z. Zheng, W. Yang, H. Wang, G. Zeng, Z. Li, S.K. Boon, P. Subbaiah, Modeling of ash formation and deposition processes in coal and biomass fired boilers: a comprehensive review, Appl. Energy 230 (Nov) (2018) 1447–1544.

[8] S. Chapela, N. Cid, J. Porteiro, J.L. Miguez, Numerical transient modelling of the fouling phenomena and its influence on thermal performance in a low-scale biomass shell boiler, Renew. Energy 161 (Dec. 2020) 309–318.

[9] S. Chapela, J. Porteiro, J.L. Miguez, F. Behrendt, Eulerian CFD fouling model for fixed bed biomass combustion systems, Fuel 278 (Oct. 2020), 118251.

[10] J.J. Rico, R. Pérez-Orozco, N. Cid, A. Larrañaga, J.L.M. Tabarés, Viability of agricultural and forestry residues as biomass fuels in the Galicia-North Portugal region: an experimental study, Sustainability 12 (Oct. 2020) 8206.

[11] A.R. Proto, A. Palma, E. Paris, S.F. Papandrea, B. Vincenti, M. Carnevale, E. Guerriero, R. Bonofiglio, F. Gallucci, Assessment of wood chip combustion and emission behavior of different agricultural biomasses, Fuel 289 (Apr. 2021), 119758.

[12] R.J. Olave, E.G.A. Forbes, C.R. Johnston, J. Relf, Particulate and gaseous emissions from different wood fuels during combustion in a small-scale biomass heating system, Atmos. Environ. 157 (May. 2017) 49–58.

[13] J. Carroll, J. Finnan, Emissions and efficiencies from the combustion of agricultural feedstock pellets using a small scale tilting grate boiler, Biosyst. Eng. 115 (May. 2013) 50–55.

[14] H. Khodaei, F. Guzzomi, G.H. Yeoh, A. Regueiro, D. Patiño, An experimental study into the effect of air staging distribution and position on emissions in a laboratory scale biomass combustor, Energy 118 (Jan) (2017) 1243–1255.

[15] A. Junejo, Y.M. Al-Abdeli, J. Porteiro, Role of primary freeboard on staged combustion of hardwood pellets in a fixed bed combustor, BioEnergy Research (Aug. 2022), https://doi.org/10.1007/s12155-022-10504-3.

[16] M. Buchmayr, J. Gruber, M. Hargassner, C. Hochenauer, Spatially resolved chemical species concentrations above the fuel bed of a small grate-fired wood-chip boiler, Biomass Bioenergy 95 (Dec) (2016) 146–156.

[17] J.P. Carroll, J.M. Finnan, F. Biedermann, T. Brunner, I. Obernberger, Air staging to reduce emissions from energy crop combustion in small scale applications, Fuel 155 (Sep. 2015) 37–43.

[18] T. Zadravec, B. Rajh, F. Kokalj, N. Samec, Influence of air staging strategies on flue gas sensible heat losses and gaseous emissions of a wood pellet boiler: an experimental study, Renew. Energy 178 (Nov. 2021) 532–548.

[19] Y. Li, Y. Lin, J. Zhao, B. Liu, T. Wang, P. Wang, H. Mao, Control of NOx emissions by air staging in small- and medium-scale biomass pellet boilers, Environ. Sci. Pollut. Control Ser. 26 (Feb. 2019) 9717–9729.

[20] H. Khodaei, F. Guzzomi, D. Patiño, B. Rashidian, G.H. Yeoh, Air staging strategies in biomass combustion-gaseous and particulate emission reduction potentials, Fuel Process. Technol. 157 (Mar. 2017) 29–41.

[21] S. Ozgen, S. Cernuschi, S. Caserini, An overview of nitrogen oxides emissions from biomass combustion for domestic heat production, Renew. Sustain. Energy Rev. 135 (Jan. 2021), 110113.

[22] A. Anca-Couce, C. Hochenauer, R. Scharler, Bioenergy technologies, uses, market and future trends with Austria as a case study, Renew. Sustain. Energy Rev. 135 (Jan. 2021), 110237.

[23] G. Archan, A. Anca-Couce, J. Gregorc, M. Buchmayr, C. Hochenauer, J. Gruber, R. Scharler, Detailed experimental investigation of the spatially distributed gas release and bed temperatures in fixed-bed biomass combustion with low oxygen concentration, Biomass Bioenergy 141 (Oct. 2020), 105725.

[24] G. Archan, R. Scharler, L. Pölzer, M. Buchmayr, P. Sommersacher, C. Hochenauer, J. Gruber, A. Anca-Couce, Detailed NOX precursor measurements within the reduction zone of a novel small-scale fuel flexible biomass combustion technology, Fuel 302 (Oct. 2021), 121073.

[25] G.A.R. Archan, R. Scharler, M. Buchmayr, N. Kienzl, C. Hochenauer, J. Gruber, A. Anca-Couce, Minimization of inorganic particulate matter emissions with a novel multi-fuel combustion technology that enhances inorganic retention in a compact updraft fixed-bed, Fuel 318 (Jun) (2022), 123611.

[26] M.M. Rahman, S. Aravindakshan, M.A. Matin, Design and performance evaluation of an inclined nozzle and combustor of a downdraft moving bed gasifier for tar reduction, Renew. Energy 172 (Jul) (2021) 239–250.

[27] M.M. Rahman, U.B. Henriksen, J. Ahrenfeldt, M.P. Arnavat, Design, construction and operation of a low-tar biomass (LTB) gasifier for power applications, Energy 204 (Aug. 2020), 117944.

[28] R. Pérez-Orozco, D. Patiño, J. Porteiro, J.L. Miguez, Bed cooling effects in solid particulate matter emissions during biomass combustion. A morphological insight, Energy 205 (Aug. 2020), 118088.

[29] A. Rezeau, L.I. Díez, J. Royo, M. Díaz-Ramírez, Efficient diagnosis of grate-fired biomass boilers by a simplified CFD-based approach, Fuel Process. Technol. 171 (Mar. 2018) 318–329.

[30] S. Somwangthanaroj, S. Fukuda, CFD modeling of biomass grate combustion using a steady-state discrete particle model (DPM) approach, Renew. Energy 148 (Apr) (2020) 363–373.

[31] T. Zadravec, C. Yin, F. Kokalj, N. Samec, B. Rajh, The impacts of different profiles of the grate inlet conditions on freeboard CFD in a waste wood-fired grate boiler, Appl. Energy 268 (Jun) (2020), 115055.

[32] R. Scharler, T. Gruber, A. Ehrenhöfer, J. Kelz, R.M. Bardar, T. Bauer, C. Hochenauer, A. Anca-Couce, Transient CFD simulation of wood log combustion in stoves, Renew. Energy 145 (Jan) (2020) 651–662.

[33] M.R. Karim, A.A. Bhuiyan, A.A.R. Sarhan, J. Naser, CFD simulation of biomass thermal conversion under air/oxy-fuel conditions in a reciprocating grate boiler, Renew. Energy 146 (Feb. 2020) 1416–1428.

[34] B. Rajh, M.A. Gómez, C. Álvarez-Bermúdez, N. Cid, J.L. Miguez, Assessment of experimental 1D and analytical 3D steady approaches of packed bed thermal conversion through the simulation of a 60-kW biomass boiler operating at half and full load, Energy Convers. Manag. 268 (Sep. 2022), 116003.

[35] M.A. Gómez, J. Porteiro, D. Patiño, J.L. Míguez, CFD modelling of thermal conversion and packed bed compaction in biomass combustion, Fuel 117 (Jan. 2014) 716–732.

[36] C. Álvarez-Bermúdez, S. Chapela, L.G. Varela, M.Á. Gómez, CFD simulation of an internally cooled biomass fixed-bed combustion plant, Resources 10 (Jul. 2021).

[37] M.A. Gómez, J. Porteiro, D. Patiño, J.L. Míguez, "Eulerian CFD modelling for biomass combustion, Transient simulation of an underfeed pellet boiler 101 (Sep. 2015) 666–680. Energy Conversion and Management.

[38] M.A. Gómez, J. Porteiro, D. de la Cuesta, D. Patiño, J.L. Míguez, Numerical simulation of the combustion process of a pellet-drop-feed boiler, Fuel 184 (Nov. 2016) 987–999.

[39] C.A. Bermúdez, J. Porteiro, L.G. Varela, S. Chapela, D. Patiño, Three-dimensional CFD simulation of a large-scale grate-fired biomass furnace, Fuel Process. Technol. 198 (Feb. 2020), 106219.

[40] A. Anca-Couce, Reaction mechanisms and multi-scale modelling of lignocellulosic biomass pyrolysis, Prog. Energy Combust. Sci. 53 (Mar. 2016) 41–79.

[41] C. Di Blasi, Modeling chemical and physical processes of wood and biomass pyrolysis, Prog. Energy Combust. Sci. 34 (Feb) (2008) 47–90.

[42] S.M. Mousavi, H. Fatehi, X.-S. Bai, Multi-region modeling of conversion of a thick biomass particle andthe surrounding gas phase reactions, Combust. Flame 237 (2022).

[43] R. Mehrabian, A. Shiehnejadhesar, R. Scharler, I. Obernberger, Multi-physics modelling of packed bed biomass combustion, Fuel 122 (Apr) (2014) 164–178.

[44] A. Dernbecher, A. Dieguez-Alonso, Advanced porous particle model in biomass pyrolysis, Chem. Eng. Trans. 92 (2022) 685–690.

[45] Z. Xia, J. Long, S. Yan, L. Bai, H. Du, C. Chen, Two-fluid simulation of moving grate waste incinerator: comparison of 2D and 3D bed models, Energy 216 (Feb. 2021), 119257.

[46] A. Anca-Couce, R. Scharler, Modelling heat of reaction in biomass pyrolysis with detailed reaction schemes, Fuel 206 (Oct. 2017) 572–579.

[47] A. Anca-Couce, P. Sommersacher, R. Scharler, Online experiments and modelling with a detailed reaction scheme of single particle biomass pyrolysis, J. Anal. Appl. Pyrol. 127 (Sep. 2017) 411–425.

[48] A. Anca-Couce, R. Mehrabian, R. Scharler, I. Obernberger, Kinetic scheme of biomass pyrolysis considering secondary charring reactions, Energy Convers. Manag. 87 (Nov. 2014) 687–696.

[49] A. Anca-Couce, I. Obernberger, Application of a detailed biomass pyrolysis kinetic scheme to hardwood and softwood torrefaction, Fuel 167 (Mar. 2016) 158–167.

[50] A. Anca-Couce, G. Archan, M. Buchmayr, M. Essl, C. Hochenauer, R. Scharler, Modelling fuel flexibility in fixed-bed biomass conversion with a low primary air ratio in an updraft configuration, Fuel 296 (Jul. 2021), 120687.

[51] M.A. Gómez, J. Porteiro, D. Patiño, J.L. Míguez, Fast-solving thermally thick model of biomass particles embedded in a CFD code for the simulation of fixed-bed burners, Energy Convers. Manag. 105 (Nov. 2015) 30–44.

[52] M.A. Gómez, J. Porteiro, D.D. la Cuesta, D. Patiño, J.L. Miguez, Dynamic simulation of a biomass domestic boiler under thermally thick considerations, Energy Convers. Manag. 140 (May. 2017) 260–272.

[53] N. Wakao, S. Kaguei, T. Funazkri, Effect of Fluid Dispersion Coefficients on Particle-To-Fluid Heat Transfer Coefficients in Packed Beds: Correlation of Nusselt Numbers, Chemical Engineering Science, 1979.
[54] N. Wakao, T. Funazkri, Effect of Fluid Dispersion Coefficients on Particle-To-Fluid Mass Transfer Coefficients in Packed Beds: Correlation of Sherwood Numbers, Chemical Engineering Science, 1978.
[55] M.A. Gómez, D. Patiño, R. Comesaña, J. Porteiro, M.A.Á. Feijoo, J.L. Míguez, CFD simulation of a solar radiation absorber, Int. J. Heat Mass Tran. 57 (Jan. 2013) 231–240.
[56] L.G. Varela, C.Á. Bermúdez, S. Chapela, J. Porteiro, J.L.M. Tabarés, Improving bed movement physics in biomass computational fluid Dynamics combustion simulations, Chem. Eng. Technol. 42 (Nov. 2019) 2556–2564.
[57] L.G. Varela, M.A. Gómez, M. Garabatos, D. Glez-Peña, J. Porteiro, Improving the bed movement physics of inclined grate biomass CFD simulations, Appl. Therm. Eng. 182 (Jan. 2021), 116043.
[58] J. Collazo, J. Porteiro, D. Patiño, E. Granada, Numerical modeling of the combustion of densified wood under fixed-bed conditions, Fuel 93 (Mar. 2012) 149–159.
[59] M.R. Karim, J. Naser, CFD modelling of combustion and associated emission of wet woody biomass in a 4 MW moving grate boiler, Fuel 222 (Jun. 2018) 656–674.
[60] A. Anca-Couce, P. Sommersacher, A. Shiehnejadhesar, R. Mehrabian, C. Hochenauer, R. Scharler, CO/CO2 ratio in biomass char oxidation, Energy Proc. 120 (Aug. 2017) 238–245.
[61] C. Di Blasi, Modeling wood gasification in a countercurrent fixed-bed reactor, AIChE J. 50 (Sep. 2004) 2306–2319.
[62] H. Thunman, B. Leckner, F. Niklasson, F. Johnsson, Combustion of wood particles—a particle model for Eulerian calculations, Combust. Flame 129 (Apr. 2002) 30–46.
[63] K.M. Bryden, K.W. Ragland, Numerical modeling of a deep and fixed bed combustor, Energy Fuels 10 (1996) 269–275.
[64] S. Chapela, J. Porteiro, M. Costa, Effect of the turbulence–chemistry interaction in packed-bed biomass combustion, Energy Fuels 31 (Aug. 2017) 9967–9982.
[65] A.G. Liden, F. Berruti, D.S. Scott, A kinetic model for the production of liquids from the flash pyrolysis of biomass, Chem. Eng. Commun. 65 (Oct) (1988) 207–221.
[66] C.K. Westbrook, F.L. Dryer, Simplified reaction mechanisms for the oxidationof hydrocarbon fuels in flames, Combust. Sci. Technol. 27 (1981) 31–43.
[67] A. Brink, Eddy Break-Up Based Models for Industrial Diffusion Flames with Complex Gas Phase Chemistry, Åbo Akademi University, 1998.
[68] F.L. Dryer, I. Glassman, High-temperature oxidation of CO and CH4, in: Symposium (International) on Combustion 14, 1973, pp. 987–1003.
[69] K. Hsu, A. Jemcov, Numerical Investigation of Detonation in Premixed Hydrogen-Air Mixture - Assessment of Simplified Chemical Mechanisms, American Institute of Aeronautics and Astronautics, 2000.
[70] A.K. Varma, A.U. Chatwani, F.V. Bracco, Studies of premixed laminar hydrogen-air flames using elementary and global kinetics models, Combust. Flame 64 (1986) 233–236.
[71] R. Pérez-Orozco, D. Patiño, J. Porteiro, N. Cid, A. Regueiro, Influence of the feeding rate on the transient behavior of a biomass combustor, Chem. Eng. Technol. 42 (Sep) (2019) 2520–2529.